Topological description of a 3D self-catenated nickel hybrid vanadate $Ni(bpe)(VO_3)_2$. Thermal stability, spectroscopic and magnetic properties†

Roberto Fernández de Luis,[a] José L. Mesa,*[b] Miren K. Urtiaga,[a] Luis Lezama,[b] María I. Arriortua[a] and Teófilo Rojo[b]

Received (in Montpellier, France) 16th January 2008, Accepted 23rd April 2008
First published as an Advance Article on the web 6th June 2008
DOI: 10.1039/b800820e

The three-dimensional $Ni(bpe)(VO_3)_2$ hybrid compound, where bpe is 1,2-di(4-pyridyl)ethene, ($C_{12}H_{10}N_2$), has been synthesized using mild hydrothermal conditions under autogeneous pressure at 140 °C during five days, obtaining green emerald prismatic single-crystals suitable for X-ray structure determination. The compound crystallizes in the orthorhombic system, space group *Pbcn*, with $a = 14.9066(5)$, $b = 7.6269(2)$ and $c = 26.9624(10)$ Å, $Z = 8$, and $R1 = 0.0373$ for 4149 observed reflections. Single-crystal X-ray diffraction reveals that the crystal structure is composed of a 3D self-catenated 10-connected uninodal net constructed from 3^6-hxl like $\{NiV_2O_6\}$ inorganic sheets linked through bpe ligands. The thermal evolution of the crystal parameters shows three different tendencies during the heating process: (i) initial contraction, (ii) thermal expansion, (iii) structural collapse due to the thermal instability of the organic ligand. The IR spectrum shows the vibrational modes of the bpe organic molecules and those of the $(VO_4)^{3-}$ tetrahedral oxoanions. Diffuse reflectance electronic absorption spectroscopy shows the characteristic bands of the Ni(II) d^8-high spin cation in slightly distorted octahedral geometry. From the positions of the bands in the electronic spectrum the *Dq* (940 cm^{-1}) and Racah, *B* (930 cm^{-1}) and *C* (3350 cm^{-1}), parameters have been calculated. Magnetic measurements indicate the existence of antiferromagnetic interactions between the Ni(II) centres of the dinuclear units, with a value of the $J/k = -59.4$, with $g = 2.076$.

1. Introduction

The construction of new organic–inorganic hybrid compounds through the rational combination of organic ligands (“spacers”), metal nodes and different anions, has become an area of great interest recently due to their potential application in catalysis, hydrogen storage, molecular adsorption, electromagnetism and photochemistry.[1]

The synergetic interaction between the organic and inorganic components allows a partial degree of “crystal engineering” by exploiting fundamental aspects of the structural organization: (i) coordination preferences and oxidation states of the metal centres. (ii) The length of the spacer, geometry, degree of flexibility and relative position of the ligand donor groups. (iii) The structural influence of the anion on the framework organization and assembly adopted by the different metal–organic moieties.

From this point of view, and in order to obtain extended hybrid frameworks, we choose Ni^{2+} due to the octahedral coordination preferences of this metal, and bidentate ligands such as pyrazine, 4,4′-bipyridine or 1,2-di(4-pyridyl)ethene. The bipyridyl ligands have very often been used since they have two nitrogen atoms that can bridge metal atoms to form polymeric compounds. These polytopic organic–amino ligands, serve to bond the metal sites and to propagate the structural information expressed by the metal coordination preferences through the extended structure.[2] The expansive chemistry of coordination polymers based on pyrazine, 4,4′-bipyridine and 1,2-di(4-pyridyl)ethene include one-, two- and three-dimensional metal–organic subnets exhibiting diamond, grid, ladder, brick, railroad and octahedral building blocks.[3]

On the other hand, the modification of the hydrothermal synthesis conditions, such as time, temperature, stoichiometry, pH, concentration and filling factor, allows a partial control of the degree of oxoanion polymerization giving rise to different stable species in solution. Examples of those are the $\{V_2O_7\}$ dimers, $\{V_4O_{12}\}$ cyclic tetramers or $\{VO_3\}$ metavanadate chains, the latter being common building blocks in first-row transition metal hybrid oxovanadium compounds. The interesting features of the metavanadate chains are the adaptability and flexibility of these structural subunits in different metal–organic environments. This is an illustrative example of the synergetic interaction between the initial structural secondary building blocks that gives rise to a great number of framework organizations in metal–organic assembly; examples include

[a] *Departamento de Mineralogía y Petrología, Facultad de Ciencia y Tecnología, Universidad del País Vasco/EHU, Apdo. 644, Bilbao, E-48080, Spain*
[b] *Departamento de Química Inorgánica, Facultad de Ciencia y Tecnología, Universidad del País Vasco/EHU, Apdo. 644, Bilbao, E-48080, Spain. E-mail: joseluis.mesa@ehu.es; Fax: +34 946013500; Tel: +34 946015523*

† Electronic supplementary information (ESI) available: S.I.-1: TGA curve, S.I.-2: PXRD patterns as a function of temperature, and S.I.-3: evolution of (002), (213) and (006) peaks as a function of temperature for $Ni(bpe)(VO_3)_2$. CCDC reference number 681328. For ESI and crystallographic data in CIF or other electronic format see DOI: 10.1039/b800820e

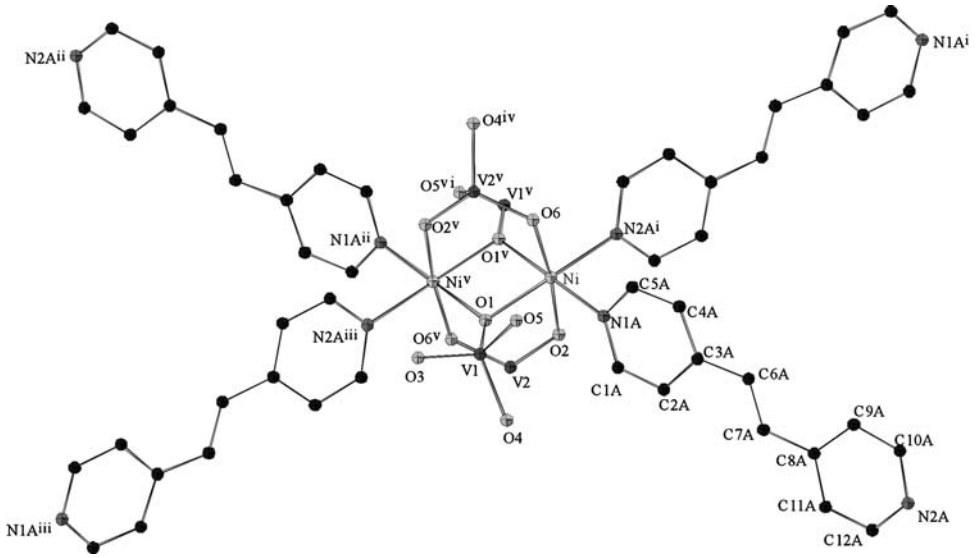

Fig. 1 A drawing of part of the Ni(bpe)$(VO_3)_2$ structure showing the coordination sphere of the vanadium and nickel atoms, and the disposition of the bpe organic ligand. (30% level of anisotropic displacements) (Symmetry codes: (i) $x - 0.5, y - 0.5, 0.5 - z$; (ii) $1 - x, -y, 1 - z$; (iii) $1.5 - x, 0.5 - y, z + 0.5$; (iv) $x - 0.5, 0.5 - y, 1 - z$; (v) $1 - x, -y, 1 - z$; (vi) $1 - x, 1 - y, 1 - z$).

$(NH_3(CH_2)_4NH_3)(VO_3)_2$, $[\{Co_2(4,4'\text{-bpy})_3(H_2O)_2\}V_4O_{12}]\cdot 2H_2O]$, $Co(bpypr)_4V_6O_{18}\cdot 2H_2O$ and $Ni(en)(VO_3)_2$.[4] Finally we have to take into account that small changes of the hydrothermal parameters have a great influence in the reaction outcome. Several pathways are available under non-equilibrium crystallization conditions but metastable kinetic phases are more likely to be isolated rather than the thermodynamic phase.

During this ongoing effort we have discovered new framework materials of unprecedented structures composed of metal organoamine coordination polymers and oxovanadium anions. Moreover, previously reported $Ni(H_2O)(pz)_{0.5}(V_4O_{12})$[5] constructed from short dipodal pyrazine ligands shows α-Po like topology ($4^{12}.6^3$-pcu) rather than the self catenated network present in the title compound.

In this work we describe the mild hydrothermal synthesis of a novel organic–inorganic hybrid compound, Ni(bpe)$(VO_3)_2$. Its low-temperature crystal structure and topological description, thermal behaviour, spectroscopic properties and magnetic behaviour are reported.

Results and discussion

Crystal structure

Single-crystal X-ray diffraction analysis reveals that the crystal structure of Ni(bpe)$(VO_3)_2$ is a three-dimensional framework constructed from edge-shared (NiN_2O_4) octahedra forming $\{Ni_2N_4O_6\}$ dinuclear units, metavanadate chains of corner-shared (VO_4) tetrahedra, and the bpe dipodal ligand directly attached to the metal centres. The connectivity between the dinuclear units and the metavanadate chains generates $\{NiV_2O_6\}$ inorganic layers parallel to the (001) plane. The bpe molecules, directly coordinated to the metal centres, act as crossed pillars between the layers. The asymmetric unit contains one nickel(II) and two vanadium(V) cations, six oxygen atoms, and one bpe organic molecule. An ORTEP drawing with the complete coordination spheres of the Ni and V atoms, and the bpe ligand is shown in Fig. 1. An interesting feature of the crystal structure is the complete disordering of the bpe ligand in two positions with occupation factors of 0.63 and 0.37, respectively. In order to simplify Fig. 1 only one of the two positions of the bpe ligand is shown.

The coordination sphere of the nickel(II) cations consists of two oxygen atoms, corner linked to vanadium tetrahedra, two nitrogen atoms in *cis* arrangement, and two O(1) atoms bridging nickel(II) metal centres. The connectivity between the nickel(II) ions and the O(1) atoms generates $\{Ni_2N_4O_6\}$ dimers constructed from edge shared octahedra (Fig. 1). The Ni–N bond lengths range from 2.087(12) for Ni(1)–N(1B) to 2.049(13) for Ni(1)–N(2B), while the Ni(1)–O bond distances, range from 2.074(2) for Ni(1)–O(1) to 2.053(2) Ni(1)–O(1)^{iii} (iii = $-x + 1, -y, -z + 1$). In this octahedron the minimum and maximum *cis*-angles are 85.7(3) and 96.3(5)°, respectively. The *trans*-angles range from 172.2(3) to 179.4(4)°. Distortion of the (NiN_2O_4) polyhedron, from an octahedron ($\Delta = 0$) to a trigonal prism ($\Delta = 1$), has been calculated by the Muetterties and Guggenberger method.[6] The value obtained of 0.0255 indicates a geometry near to ideal octahedral.

Each $\{Ni_2N_4O_6\}$ dimer is connected *via* (VO_4) tetrahedra to other six similar nodes in the same plane, stabilising a 3^6 "hxl" hexagonal lattice-like connectivity in the $\{NiV_2O_6\}$ inorganic layer (Fig. 2(a)). The bpe ligand is directly coordinated to the metal centre and acts as a pillar between the inorganic sheets (Fig. 2(b)). In this way, each node in the same plane is connected, *via* the organic ligand, to four others, two belonging to the above layer and other two to the below layer (Fig. 2(a)). The connectivity between the inorganic layers and the bpe ligand generates an ABABAB stacking of the layers along the [001] direction. The simplified network[7,8] is a 10-c uninodal net with a Schlafli notation of $\{3^6.4^{31}.5^6.6^2\}$. Moreover, the connectivity between inorganic layers through

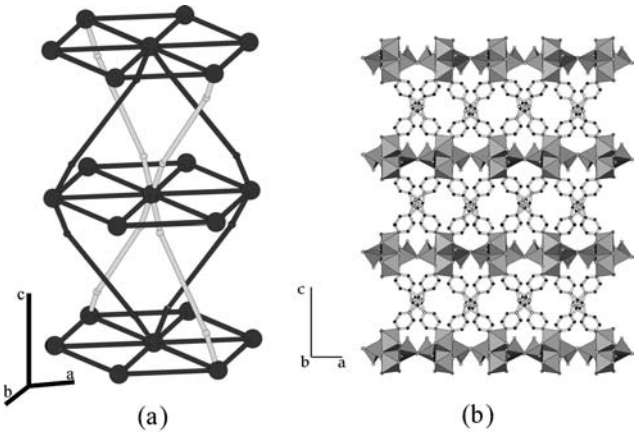

Fig. 2 (a) Topological description of the 3D self-catenated 10-connected uninodal network. The nodes represents the dinuclear units $\{Ni_2N_4O_6\}$. (b) 3D Structure constructed from $\{NiV_2O_6\}$ inorganic layers pillared by bpe ligands.

the bpe ligand generates a self-penetrating network. In this way the shortest rings constructed from $\{Ni_2N_4O_6\}$ nodes and bpe ligands are catenated by the bpe ligand of other node–bpe shortest rings of the same network (Fig. 2(a)).

The asymmetric unit shows that there are two crystallographically independent vanadium cations V(1) and V(2), which are corner shared by O(4) and O(5) forming the metavanadate chains. Both V(1) and V(2) sites are covalently attached: the V(1) binds one $\{Ni_2N_4O_6\}$ octahedral dimer through the O(1) atom whereas the V(2) atom is corner linked to one $\{Ni_2N_4O_6\}$ dinuclear unit through O(2) and O(6) atoms. Consequently, the terminal vanadyl (V═O) group is found only in the V(1) site. The oxygen atoms shared by two adjacent $(VO_4)^{3-}$ tetrahedra have V–O bond lengths[9] ranging from 1.787(2) Å for V(1)–O(4) to 1.801(2) Å for V(2)–O(5)^{v} (v = x, y + 1, z). The oxygen atoms corner-shared by the vanadium tetrahedra and the $\{Ni_2N_4O_6\}$ octahedral dimers have shorter bond distances, ranging from 1.654(2) Å for V(2)–O(6)^{iii} (iii = $-x$ + 1, $-y$, $-z$ + 1) to 1.717(2) Å for V(1)–O(1). The terminal vanadyl (V1(1)═O(3)) group has the shortest V–O bond length with a value of 1.605(2) Å. In both tetrahedral oxoanions the O–V–O bond angles range from 107.25(9) to 111.19(9)°. The bond valance calculation,[10] assuming V^{v}–O bonds, gives charge values of 5.13 v.u. for V(1), 5.10 v.u. for V(2) and 2.045 v.u. for the Ni(1) atom.

The $\{VO_3\}_n^{n-}$ chains consist of one-dimensional folded chains of corner sharing (VO_4) tetrahedra, which extends parallel to the *b* axis. These tetrahedra are common building blocks in secondary metal–ligand vanadium oxides, such as $(NH_3(CH_2)_4NH_3)(VO_3)_2$, $M(Hdpa)V_4O_{12}$ (M = Ni, Co), $Cu(2,2'\text{-bpy})V_2O_6$, $Co(bpypr)_4V_6O_{18}\cdot 2H_2O$ and $Ni(en)(VO_3)_2$,[4,11] however, the connectivity between the metal centres and the $\{VO_3\}_n^{n-}$ chains in these vanadates are different. On the other hand, the variability of the V–O distances and V–O–V angles allows relative movements and rotations of the adjacent tetrahedra in the chains. This fact indicates that the metavanadate chains can adapt their geometry to the different metal–organic subnets $Cu(dpa)VO_3$, $Cu(tn)_2(VO_3)_2$.[11]

The crystal structure of the previously reported $Ni(H_2O)(pz)_{0.5}(V_4O_{12})$[5] is constructed from inorganic layers pillared by pz ligand. Further, similar dimeric units are present in the inorganic layers, linked through $\{V_4O_{12}\}$ cyclic units. The parallel disposition of the ligand between the layers, and the connectivity of the dinuclear units through the vanadium tetrahedral generates an α-Po like topology ($4^{12}.6^3$-pcu) without any interpenetration or self-catenation of the network. Taking this fact into account, the length of the bpe organic linker, in comparison with the pz one, could provide more opened windows in the structure that allows the self-catenation of the network in order to provide a better packing of the whole structure.

Thermal behaviour

The thermogravimetric curve of this phase exhibits two steps of weight loss. The first one, with a value of 1.5% between room temperature and 70 °C, corresponds to the loss of adsorbed water, and the second one, with a value of 40.8% in the temperature range 400–460 °C, corresponds to the exothermic loss of bpe. The whole weight loss is in agreement with the value calculated (41.5%) for the decomposition of the compound after calcination of the organic molecules (ESI,† Fig. S.I.-1).

The thermal behaviour of $Ni(bpe)(VO_3)_2$ was also studied by time-resolved X-ray thermodiffractometry in air atmosphere. The thermodiffractometric analysis reveals that the title compound is stable from room temperature to 445 °C, but the crystallinity decreases dramatically by 385 °C (ESI,† Fig. S.I.-2). A previous analysis of the pattern shows the existence of significant displacements of some reflections such as (002), (213) and (006) (ESI,† Fig. S.I.-3).

The Rietveld cyclic refinement of the crystal parameters with respect to temperature shows the thermal behaviour of the $Ni(bpe)(VO_3)_2$ phase. Owing to the preferred orientation of the sample there are problems in the fit of some reflection intensities. The introduction of a fixed structural model during the cyclic refinement of the crystal parameters allows a better description of the thermal behaviour. The relative expansion has been calculated using the following equation: R.E.(%) = $[(P_{t(i)}/P_{t(0)}) - 1] \times 100$, where, $P_{t(i)}$ and $P_{t\,(0)}$ are the parameter values at $t = i$ and 0 °C, respectively. In order to establish a quantitative comparison between the evolution of the crystal parameters and cell volume with temperature we have plotted these in Fig. 3(a)–(d).

The evolution of the cell parameters with temperature suggests three different tendencies in the crystal structure during the heating process: initial contraction, structural expansion and structural collapse. The values of the crystal parameters, at initial temperature, after the structural contraction (t = 90 °C) and thermal expansion (t = 315 °C), and before the structural collapse (t = 390 °C), are presented in Fig. 3(a)–(d). It can be seen that the different stages are: (i) structural contraction between room temperature and 90 °C. This structural contraction is shown in the reduction of the *b* and *c* parameters between 30 and 90 °C, $b_{(30)}$ = 7.637(2) Å → $b_{(90)}$ = 7.618(1) Å and $c_{(30)}$ = 26.982(2) Å → $c_{(90)}$ = 26.951(2) Å, respectively. (ii) Thermal expansion of the structure between 90 and 315 °C. The volume

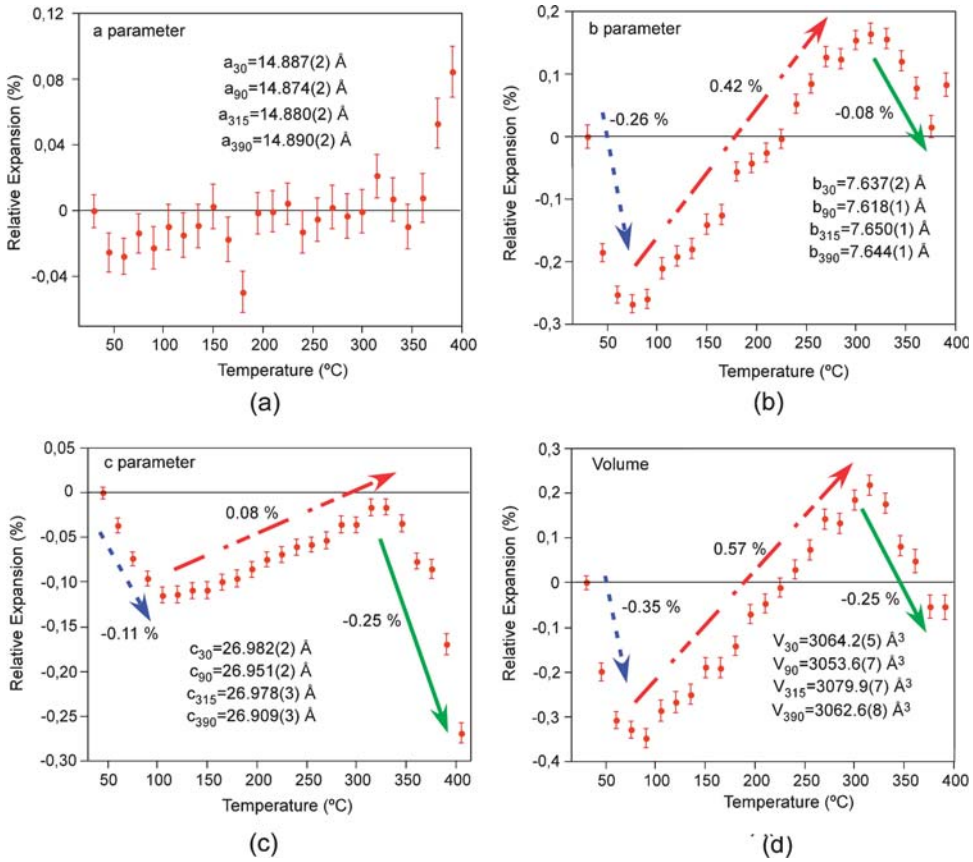

Fig. 3 Thermal behaviour of Ni(bpe)$(VO_3)_2$. Relative expansion (%) of the crystal parameters and cell volume with temperature.

of the unit cell increases by +0.55% in this range of temperatures. The evolution of the crystal parameters suggests an increase in the interlayer distance ($c_{(90)}$ = 26.951(2) Å → $c_{(315)}$ = 26.978(3) Å) and expansion of the inorganic layers in the [010] direction (($b_{(90)}$ = 7.618(1) Å → $b_{(315)}$ = 7.650(1) Å), which is in the same direction of the metavanadate chains. (iii) Structure collapse between 315 and 445 °C. The loss of the crystallinity hinders the refinement of the patterns above 390 °C. Apparently the most intense reflections (002), (004) and (006) move to higher values of 2θ. This fact suggests a shortening in the interlayer space (*c* parameter ($c_{(315)}$ = 26.978(3) Å → $c_{(390)}$ = 26.909(3) Å)) between the inorganic layers due to the thermal instability of the organic ligand, and finally the structural collapse. Also there is a contraction in the inorganic layers in the [010] direction (($b_{(315)}$ = 7.650(1) Å → $b_{(390)}$ = 7.644(1) Å).

The thermal response of the crystal structure is strongly dependent on the *b* and *c* crystal parameters. In this respect, the relative expansion of the *b* parameter is, approximately, twice that of *c*, during the structural contraction. In the same way, during the thermal expansion the *b* parameter increases its value by 0.42% while the *c* parameter has a relative expansion of 0.08% (Fig. 3(a)–(d)). This fact suggest that the thermal expansion is strongly correlated with the expansion of the inorganic sheets along the [010] direction. In contrast with these two first steps, the structural collapse due to the instability of the organic ligand is in good agreement with the reduction of the *c* parameter, −0.25% (Fig. 3(c)), while the lower relative expansion of the *b* parameter, 0.08% (Fig. 3(b)), is related to the more stable inorganic sheets. During the heating process the *a* parameter remains practically unchanged (Fig. 3(a)). Previously published metal–organic polymers[12] shows large values of negative thermal expansion related to the tilting of the organic linkers. The initial structural contraction of the title compound may be related to a progressive tilting of the bpe linkers. This process could explain the *b* and *c* parameter evolution.

The maxima observed in the diffractograms recorded in the 445–610 °C range showed that the calcination products are NiV_2O_6 [$P\bar{1}$, a = 7.130, b = 4.791, c = 8.825 Å, α = 90.16, β = 102.13, γ = 94.19°][13a] and V_2O_5 [$Pmn2_1$, a = 11.503, b = 4.309, c = 3.557 Å].[13b] Above this temperature, in the 610–665 °C range the vanadium oxide V_2O_5 together with two unidentified maxima at 23.7 and 28.1° are observed. The same mixture is observed in the pattern recorded at 25 °C after the heating process.

IR and UV-Vis spectroscopies

The IR spectrum of Ni(bpe)$(VO_3)_2$ shows the bands corresponding to the vibrational modes of the bpe organic molecule and $(VO_4)^{3-}$ vanadate anions, which appear in the 1600–990 and 930–530 cm^{-1}, ranges, respectively. The characteristic bands of the bpe molecule, δ(ring), δ(C=N) and δ(C=C), appear at 990, 1550, 1610 cm^{-1} respectively.[14]

In the diffuse reflectance spectrum, two absorption bands of strong intensity corresponding to the allowed transitions: $^3A_{2g}(^3F)$

$\rightarrow {}^3T_{2g}({}^3F)$, $^3T_{1g}({}^3F)$, at 9400 and 15 500 cm^{-1}, and the forbidden one $^3A_{2g}({}^3F) \rightarrow {}^1E_{1g}(D)$ at 12 250 cm^{-1}, are observed. From the spin transitions corresponding to the d^8-high spin Ni(II) cation in octahedral geometry, the Dq and Racah B and C parameters have been calculated, by using the energy expressions given in the Tanabe–Sugano diagrams.[15] The values are $Dq = 940$, $B = 930$ cm^{-1} and $C = 3350$ cm^{-1}. The value of the B-parameter is, approximately, 90% of that of the free Ni(II) cation (1030 cm^{-1}), which indicates an appreciable covalent character in the chemical bonds for the $\{NiN_2O_4\}$ octahedron.

Magnetic behaviour

Magnetic measurements for the Ni(bpe)$(VO_3)_2$ phase were performed on a powdered sample from room temperature to 2.0 K, at a magnetic field of 0.1 T. The thermal evolution of the molar magnetic susceptibility, χ_m, and of $\chi_m T$ *vs.* T is shown in Fig. 4. For Ni(bpe)$(VO_3)_2$ the $\chi_m T$ value at 300 K is close to the spin-only (1.00 cm^3 K mol^{-1}) expected for non-interacting Ni(II) ($S = 1$) ions. The molar susceptibility, χ_m, slightly increases with decreasing temperature and shows a broad maximum at 100 K. After passing through the maximum the χ_m value slightly decreases to 0.0032 emu mol^{-1} at 20 K. At lower temperatures the curve increases abruptly to reach 0.0144 emu mol^{-1} at 2 K.

The temperature dependence of the χ_m curve between 300 and 20 K is typical of an intradimer antiferromagnetic interaction, because the distances between the adjacent dimers are considerably longer than the intradimer M1···M2 separation (2.9886(6) Å). The increase of the χ_m values at lower temperatures can be attributed to a small portion of a Ni(II) paramagnetic impurity.

The intradimer antiferromagnetic interaction can be treated with the isotropic spin Hamiltonian $H = -2JS_AS_B$.[16] The molar magnetic susceptibility for a Ni(II) dimer (local spins $S_A = S_B = 1$) may be expressed by eqn (1):

$$\chi_m = \frac{2N\beta^2g^2}{kT}\frac{1+5\exp(4x)}{3+5\exp(4x)+\exp(-2x)}(1-\rho) + \frac{2N\beta^2g^2}{kT}\frac{(2/y)-((2\exp(-y)/y)+\exp(-y)}{1+2(\exp(-y))}\rho + \mathrm{TIP} \quad (1)$$

$$x = J/kT;\ y = D/kT$$

where N is Avogadro's number; β, Bohr magneton; g, gyromagnetic ratio; k, Bolzmann's constant; T, absolute temperature; ρ, impurity percentage and TIP, temperature independent paramagnetism. The second term takes into account a minor Ni(II) paramagnetic impurity (100ρ%) at low temperatures, and the last term is the temperature independent paramagnetism (TIP). Although Ni(II) in an axial symmetry can have a large zero-field splitting, the magnetic behaviour of Ni(II) dimers closely follows eqn (1) when a relatively strong antiferromagnetic interaction is operative, which makes the consideration of $D_{Ni(II)\ dimer}$ unnecessary. The best fitting parameters obtained are $J/k = -59.4$ K, $g = 2.076$, $\rho = 0.0435$ (4.35%), $D_{Ni(II)\ impurity}/k = 6.85$ K, TIP = 0.00076, with a value of the residual factor $R = \sum[\chi_{m(exp)} - \chi_{m(calc)}]^2/\sum[\chi_{m(exp)}]^2$ of 2.5×10^{-4}. These values are consistent with the existence of antiferromagnetically coupled dinuclear Ni(II) centers.

In a second approach to describe the magnetic behaviour of Ni(bpe)$(VO_3)_2$ we introduce the zero field splitting parameter of the Ni(II) dinuclear cores (D_{dimer}). The best fit still gives a poor fit in the broad maximum at 100 K.

The antiferromagnetic behaviour of the title compound is closely related to those observed in several octahedrally coordinated Ni(II) complexes with similar binuclear cores. Most of the magneto–structural correlations for dinuclear Ni(II) complexes are based on the work of Nanda *et al.*[17] This work indicates a linear relationship between J and Ni–O–Ni bridging angle in Ni(II) dimers. Furthermore, a bridging angle of 97° is the crossover point between ferromagnetic and antiferromagnetic coupling. On the other hand, Cano *et al.*[18] have suggested that the out of plane angle (ϕ) is of as much importance as M–X–M angle (θ) in determining the sign and direction of the exchange value. From this point of view the Ni–O–Ni angle in Ni(bpe)$(VO_3)_2$ with values of 92.79(7) and 87.21(7)° values may favour ferromagnetic interaction between the magnetic centres, but the out of plane angles Ni–O–V(1), 127.55(10) and 135.64(10)°, and the connectivity of the Ni(II) cations with the V(2) atoms have a great influence in the final magnetic behaviour, allowing the antiferromagnetic behaviour observed in the susceptibility measurements.

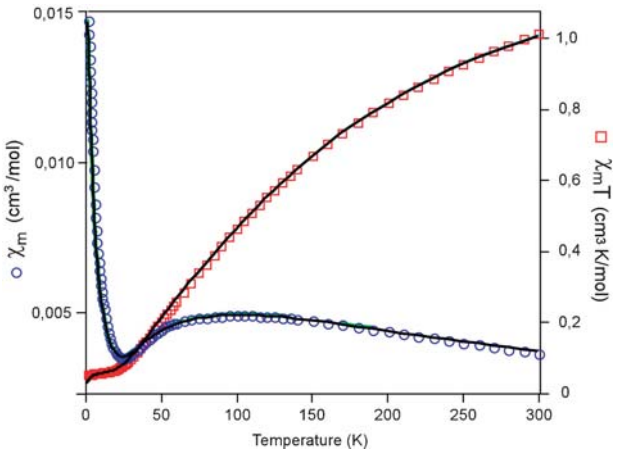

Fig. 4 Plot of χ_m (circles) and $\chi_m T$ (squares) *vs.* temperature. The solid lines represent the best fit assuming an intradimer antiferromagnetic interaction and a minor amount of zero-field split Ni(II) paramagnetic impurity.

Experimental

Synthesis and characterization

Ni(bpe)$(VO_3)_2$, where bpe is 1,2-di(4-pyridyl)ethene, was synthesized by using mild hydrothermal conditions under autogeneous pressure. The hydrothermal reaction of a mixture of $Ni(NO_3)_2{\cdot}6H_2O$ (150 mg; 0.516 mmol), $Na(VO_3)$

(0.1258 mg; 1.025 mmol), bpe ($C_{12}H_{10}N_2$) (0.0944 mg; 0.5148 mmol), and H_2O (30 mL) at 140 °C during five days results in green emerald prismatic crystals of the title compound. The initial pH of the reaction was 6, which did not show change during the hydrothermal treatment. The crystalline mixture was washed thoroughly with methanol and deionized water and dried in air at room temperature.

The atomic percentages of the elements in the $Ni(C_{12}H_{10}N_2)(VO_3)_2$ phase was calculated by atomic absorption spectroscopy (AAS) and C, N, H elemental analysis. Found: Ni, 13.35; V, 23.19; C, 32.79; N, 6.34; H, 2.26; required: Ni, 13.37; V, 23.22; C, 32.81; N, 6.38; H, 2.28%. The density, 1.89(2) g cm^{-3}, was measured by the flotation method in a mixture of bromoform–chloroform being, .

The phase was characterized by X-ray powder diffraction data. The crystal X-ray diffraction unit cell-parameters were refined with the pattern matching routine of the FULLPROF program,[19] giving the following results: a = 14.838(1), b = 7.6331(7), c = 26.922(2) Å. The parameters are similar to those obtained from the single-crystal structural resolution, a = 14.9066(5), b = 7.6269(2), c = 26.9624(10) Å, indicating high chemical purity and crystallinity of the different samples.

Single-crystal X-ray diffraction

A block like single-crystal with dimensions given in Table 1, was selected under a polarising microscope and mounted on a glass fibre. Single-crystal X-ray diffraction data were collected at 150 K on an STOE IPDS (Imaging Plate Diffraction System) automatic diffractometer (Mo-Kα radiation). Details of crystal data and some features of the structure refinement are reported in Table 1. Lattice constants were obtained by using a standard program belonging to the software of the diffractometer, confirming at the same time the good quality of the single-crystal.

Lorentz-polarization and absorption corrections were made with the diffractometer software, taking into account the size and shape of the crystals.[20] The structures were solved by direct methods (SHELXS86)[21] in the orthorhombic *Pbcn* space group, which allowed to obtain the positions of the Ni(II) and V(V) ions. The refinement of the crystal structures was performed by full-matrix least squares based on F^2, using the SHELXL97 program,[22] obtaining the oxygen, carbon and nitrogen atoms. Scattering factors were taken from ref. 23. Anisotropic thermal parameters were used for all atoms except the hydrogen ones belonging to the organic molecule which were fixed geometrically and allowed to ride on their parent carbon atoms (C–H 0.93 Å) and refined with common isotropic displacements. The bpe molecule was statically disordered in two positions with occupation factors near 0.63/0.37. The disorder was solved assuming equivalence of the chemical equivalent bond lengths and angles, but not torsion angles, of the two disordered bpe molecules. For this purpose the SAME, PART, SIMU and SADI commands available in SHELXL97 were used. Equal anisotropic thermal displacements were used for the carbon and nitrogen atoms belonging to the disordered bpe molecules in order to avoid unusual thermal ellipsoids in the disordered carbon atoms with short distances. In the final stages of the refinement the Ni–N1A, Ni–N1B and Ni–N2A, Ni–N2B bonds were treated as chemically equivalent. Final *R*-factors are given in Table 1, together with the maximum and minimum peaks in the final Fourier differences synthesis, and the goodness of the fit. Simulation based on the crystal structure of this phase was in excellent agreement with the X-ray powder data, indicating the presence of a pure compound with high crystallinity. Table 2 shows the selected bond distances and angles.

Table 1 Crystal data and structure refinement for $Ni(bpe)(VO_3)_2$

Formula	$C_{12}H_{10}N_2NiV_2O_6$
M_r/g mol^{-1}	438.81
Crystal system	Orthorhombic
Space group	*Pbcn*
a/Å	14.9066(5)
b/Å	7.6269(2)
c/Å	26.9624(10)
Z, $F(000)$, T/K	8, 1744, 150
μ/mm^{-1}	2.44
D_c, D_m/g cm^{-3}	1.902, 1.89(2)
Crystal size/mm	0.25 × 0.11 × 0.09
Crystal colour	Green
Radiation (λ/Å)	0.71073
No. of reflns., Indep. reflns.	4149, 3120
h,k,l range	−20 to 17, −10 to 10, −36 to 36
R_{int}, R_{sigma}	0.0521, 0.0398
Programs	SHELXS86, SHELXL97
$R1$, $wR2$(obs) ($I > 2\sigma(I)$)	0.0387, 0.0906
$R1$, $wR2$(all)	0.0585, 0.0952
GooF, S	0.976
No. parameters/restraints	191, 447
$\Delta\rho_{max,\ min}$/e $Å^{-3}$	1.514, −0.934

Physical measurements

The IR spectrum (KBr pellet) were obtained with a Nicolet FT-IR 740 spectrophotometer in the 400–4000 cm^{-1} range. The diffuse reflectance spectrum was registered at room temperature on a Cary 5000 spectrophotometer in the 210–2000 nm range. Thermogravimetric analysis was carried out under air in a DSC 2960 Simultaneous DSC-TGA TA Instrument. A crucible containing *ca.* 7 mg of the sample was heated at 5 °C min^{-1} in the temperature range 30–500 °C. The final temperature of this thermal analysis was increased only up to 500 °C, because at higher temperature the vanadium metal diffuses into the small pores of the alumina crucible. Temperature-dependent PXRD measurements in air atmosphere was realized in a PHILIPS X'PERT automatic diffractometer (Cu-Kα radiation) equipped with a variable-temperature stage (Paar Physica TCU2000) with Pt sample holder. An initial powder pattern was recorded at room temperature in 2θ steps of 0.03° in the range 5 ≤ 2θ ≤ 41°, in order to use the Pt (111) maxima, 2θ = 39°, as calibrant to measure the initial sample displacement. At higher temperatures, the powder patterns were recorded in 2θ steps of 0.03° in the range 5 ≤ 2θ ≤ 35°, counting for 1 s per step and increasing the temperature at 5 °C min^{-1} from room temperature up to 665 °C. Finally, a powder pattern was recorded at room temperature after the calcination of the sample. Magnetic measurements on powdered samples were performed in the temperature range 2–300 K, using a Quantum Design MPMS-7 SQUID magnetometer. The magnetic field was 0.1 T, a value in the range of linear dependence of magnetization *vs.* magnetic field, even at 2.0 K.

Table 2 Selected bond length (Å) and angles (°) for Ni(bpe)$(VO_3)_2$

N(1A)-Ni(1)	2.077(8)	O(2)–V(2)	1.6604(19)
N(1B)–Ni(1)	2.087(12)	O(3)–V(1)	1.605(2)
N(2A)–Ni(1)#1	2.080(8)	O(4)–V(2)#4	1.787(2)
N(2B)–Ni(1)#1	2.049(13)	O(4)–V(1)	1.787(2)
Ni(1)–O(1)#3	2.0530(18)	O(5)–V(1)	1.785(2)
Ni(1)–O(6)	2.0554(19)	O(5)–V(2)#5	1.801(2)
Ni(1)–O(2)	2.0644(18)	O(6)–V(2)#3	1.654(2)
Ni(1)–O(1)	2.0742(17)	V(2)–O(6)#3	1.654(2)
Ni(1)–N(2A)#2	2.080(8)	V(2)–O(4)#6	1.787(2)
O(1)–V(1)	1.7166(18)	V(2)–O(5)#7	1.801(2)
N(2B)#2–Ni(1)–O(1)#3	94.3(7)	O(2)–Ni(1)–N(1B)	85.7(3)
N(2B)#2–Ni(1)–O(6)	88.8(5)	O(1)–Ni(1)–N(1B)	93.1(4)
O(1)#3–Ni(1)–O(6)	87.26(8)	V(1)–O(1)–Ni(1)#3	135.64(10)
N(2B)#2–Ni(1)–O(2)	96.3(5)	V(1)–O(1)–Ni(1)	127.55(10)
O(1)#3–Ni(1)–O(2)	86.59(7)	Ni(1)#3–O(1)–Ni(1)	92.79(7)
O(6)–Ni(1)–O(2)	172.33(8)	V(2)–O(2)–Ni(1)	127.92(10)
N(2B)#2–Ni(1)–O(1)	175.6(7)	V(2)#4–O(4)–V(1)	158.10(15)
O(1)#3–Ni(1)–O(1)	87.21(7)	V(1)–O(5)–V(2)#5	127.48(11)
O(6)–Ni(1)–O(1)	87.18(7)	V(2)#3–O(6)–Ni(1)	128.66(11)
O(2)–Ni(1)–O(1)	87.95(7)	O(3)–V(1)–O(1)	109.57(10)
O(1)#3–Ni(1)–N(1A)	178.8(2)	O(3)–V(1)–O(5)	108.45(11)
O(6)–Ni(1)–N(1A)	91.75(19)	O(1)–V(1)–O(5)	111.19(9)
O(2)–Ni(1)–N(1A)	94.35(19)	O(3)–V(1)–O(4)	108.98(12)
O(1)–Ni(1)–N(1A)	92.1(3)	O(1)–V(1)–O(4)	110.67(9)
O(1)#3–Ni(1)–N(2A)#2	92.2(4)	O(5)–V(1)–O(4)	107.92(10)
O(6)–Ni(1)–N(2A)#2	92.8(3)	O(6)#3–V(2)–O(2)	110.03(9)
O(2)–Ni(1)–N(2A)#2	92.0(3)	O(6)#3–V(2)–O(4)#6	110.73(11)
O(1)–Ni(1)–N(2A)#2	179.4(4)	O(2)–V(2)–O(4)#6	108.78(10)
N(1A)–Ni(1)-N(2A)#2	88.5(6)	O(6)#3–V(2)–O(5)#7	111.19(10)
N(2B)#2–Ni(1)–N(1B)	85.9(9)	O(2)–V(2)–O(5)#7	108.78(9)
O(1)#3–Ni(1)–N(1B)	172.2(3)	O(4)#6–V(2)–O(5)#7	107.25(9)
O(6)–Ni(1)–N(1B)	100.5(3)		

Symmetry transformations used to generate equivalent atoms: #1 $x + 1/2, y + 1/2, -z + 1/2$; #2 $x - 1/2, y - 1/2, -z + 1/2$; #3 $-x + 1, -y, -z + 1$; #4 $-x + 3/2, y + 1/2, z$; #5 $x, y + 1, z$; #6 $-x + 3/2, y - 1/2, z$; #7 $x, y - 1, z$.

Concluding remarks

The Ni(bpe)$(VO_3)_2$ phase has a three-dimensional structure constructed from inorganic layers pillared by the bpe ligand. The topological analysis of the net shows a self-catenation in a 10-c uninodal net with a Schlafli symbol of $\{3^6.4^{31}.5^6.6^2\}$. The thermal behaviour of Ni(bpe)$(VO_3)_2$ shows that the structural organization confers some degree of flexibility to the whole framework, giving rise to three different tendencies during the heating process: structure contraction—thermal expansion—structure collapse. Finally, the connectivity between the nickel(II) centers in the dinuclear cores originates an antiferromagnetic behaviour, which has been parameterized to obtain, $J/k = -59.4$, $g = 2.076$, $p = 0.0435$ (4.35%), $D_{\mathrm{Ni(II)\ impurity}}/k = 6.85$ K, TIP = 0.00076.

Acknowledgements

This work has been financially supported by the "Ministerio de Educación y Ciencia" (MAT2007-60400) and the "Gobierno Vasco" (IT-177-07 and IT-312-07), which we gratefully acknowledge. The authors thank the technicians of SGIker, Drs J. Sangüesa, I. Orue, P. Vitoria and A. Larrañaga, financed by the National Program for the Promotion of Human Resources within the National Plan of Scientific Research, Development and Innovation, "Ministerio de Ciencia y Tecnología" and "Fondo Social Europeo" (FSE), for the X-ray diffraction and magnetic measurements, respectively. R. Fernández de Luis thanks the MEC (Madrid, España) for funding.

References

1 S. Kitagawa, R. Kitaura and S.-I. Noro, *Angew. Chem., Int. Ed.*, 2004, **43**, 2334.
2 P. J. Hargman, D. Hargman and J. Zubieta, *Angew. Chem., Int. Ed.*, 1999, **38**, 2638.
3 V. A. Blatov, L. Carlucci, G. Ciani and D. M. Proserpio, *CrystEngComm*, 2004, **6**, 377.
4 (*a*) D. Riou and G. Férey, *J. Solid State Chem.*, 1996, **124**, 151; (*b*) M. I. Khan, E. Yohannes, R. C. Nome, S. Ayesh, V. O. Golub, C. J. O'Connor and R. J. Doedens, *Chem. Mater.*, 2004, **16**, 5273; (*c*) R. L. La Duca, R. Ratkosky, R. S. Rarig, J. Zubieta and C. O'Connor, *J. Solid State Chem.*, 1996, **122**, 251; (*d*) L. Shi-Xiong, L. Bi-Zhou and L. Shen, *Inorg. Chim. Acta*, 2004, **304**, 33.
5 E. S. Larrea, J. L. Mesa, J. L. Pizarro, M. I. Arriortua and T. Rojo, *J. Solid State Chem.*, 2007, **180**, 1149.
6 E. L. Muetterties and L. J. Guggenberger, *J. Am. Chem. Soc.*, 1974, **96**, 1748.
7 (*a*) O. Delgado-Friedrichs, M. O'Keeffe and O. M. Yaghi, *Acta Crystallogr., Sect. A: Found. Crystallogr.*, 2003, **59**, 22; (*b*) O. Delgado-Friedrichs and M. O'Keeffe, *J. Solid State Chem.*, 2005, **178**, 2480; (*c*) http://www.topos.ssu.samara.ru; A. V. Blatov, *IUCr CompComm. Newslett.*, 2006, **7**, 4.
8 (*a*) L. Carlucci, G. Ciani and D. M. Proserpio, *Coord. Chem. Rev.*, 2003, **246**, 247; (*b*) S. R. Batten, *CrystEngComm*, 2001, **18**, 1.
9 P. Y. Zavalij and M. S. Whittingham, *Acta Crystallogr., Sect. B: Struct. Sci.*, 1999, **55**, 627.
10 I. D. Brown, in *Structure and Bonding in Crystals*, ed. M. O'Keeffe and A. Navrotsky, Academic Press, New York, 1981, vol. 2, p. 1.
11 (*a*) R. L. La Duca, R. S. Rarig and J. Zubieta, *Inorg. Chem.*, 2001, **40**, 607; (*b*) P. J. Hargman and J. Zubieta, *Inorg. Chem.*, 2001, **40**,

2800; (*c*) R. L. La Duca, R. Finn and J. Zubieta, *Chem. Commun*., 1999, 1669; (*d*) L. Bi-Zhou and L. Shi-Xiong, *Polyhedron*, 2000, **19**, 2521.
12 (*a*) C. J. Kepert, *Chem. Commun*., 2006, 695; (*b*) S. S. Han and W. A. Goddard, *J. Phys. Chem. C*, 2007, **111**, 15185.
13 Powder Diffraction File—Inorganic and Organic: (a) 01-080-1149; (b) 022-0454.
14 K. Nakamoto, *Infrared Spectra of Inorganic and Coordination Compounds*, Wiley, New York, 1986.
15 (*a*) A. B. P. Lever, *Inorganic Electronic Spectroscopy*, Elsevier Science Publishers B.V., Amsterdam, Netherlands, 1984; (*b*) T. Y. Sugano, *J. Phys. Soc. Jpn*., 1954, **9**, 753.
16 R. L. Carlin, *Magnetochemistry*, Springer-Verlag, Berlin, 1986.
17 K. K. Nanda, L. K. Thompson, J. N. Bridson and K. Nag, *J. Chem. Soc., Chem. Commun*., 1994, 1337.
18 (*a*) M.-H. Zeng, B. Wang, X.-Y. Wang, W.-X. Zhang, X.-M. Chen and S. Gao, *Inorg. Chem*., 2006, **45**, 7069; (*b*) J. Cano, G. De Mundo, J. L. Sanz, R. Ruiz, J. Faus, F. Loret, M. Julve and A. Caneschi, *J. Chem. Soc., Dalton Trans*., 1997, 1915; (*c*) S. K. Dey, M. S. El Fallah, J. Ribas, T. Matsushita, V. Gramlich and S. Mitra, *Inorg. Chim. Acta*, 2004, **357**, 1517; (*d*) P. Vitoria, I. Muga, J. M. Gutierrez-Zorrilla, A. Luque, P. Román, L. Lezama, F. J. Zuñiga and J. I. Beitia, *Inorg. Chem*., 2003, **42**, 960.
19 J. Rodríguez-Carvajal, FULLPROF98, *Program for Rietveld Pattern Matching Analysis of Powder Patterns*, Grenoble, 1998, unpublished work.
20 W. Yingua, *J. Appl. Crystallogr*., 1987, **20**, 258.
21 G. M. Sheldrick, *SHELXS86: Program for the Solution of Crystal Structures*, University of Göttingen, Germany, 1986.
22 G. M. Sheldrick, *SHELXL97: Program for the Refinement of Crystal Structures*, University of Göttingen, Germany, 1997.
23 *International Tables for X-ray Crystallography*, Kynoch Press, Birmingham, UK, 1974, vol. VI, p. 99.